INSTITUTE OF PHYSICS PUBLISHING BIOINSPIRATION & BIOMIMETICS
Bioinsp. Biomim. **1** (2006) S19–S24 doi:10.1088/1748-3182/1/4/S03

Numerical simulations of undulatory swimming at moderate Reynolds number

Jeff D Eldredge

Mechanical & Aerospace Engineering Department, University of California, Los Angeles, CA 90095, USA

E-mail: eldredge@seas.ucla.edu

Received 27 July 2006
Accepted for publication 9 November 2006
Published 22 December 2006
Online at stacks.iop.org/BB/1/S19

Abstract
We perform numerical simulations of the swimming of a three-linkage articulated system in a moderately viscous regime. The computational methodology focuses on the creation, diffusion and transport of vorticity from the surface of the bodies into the fluid. The simulations are dynamically coupled, in that the motion of the three-linkage swimmer is computed simultaneously with the dynamics of the fluid. The novel coupling scheme presented in this work is the first to exploit the relationship between vorticity creation and body dynamics. The locomotion of the system, when subject to undulatory inputs of the hinges, is computed at Reynolds numbers of 200 and 1000. It is found that the forward swimming speed increases with the Reynolds number, and that in both cases the swimming is slower than in an inviscid medium. The vortex shedding is examined, and found to exhibit behavior consistent with experimental flow visualizations of fish.

1. Introduction

The undulatory mode of locomotion predominates in aquatic organisms over an enormous range of Reynolds numbers, from the flagellar propulsion of spermatozoa to the carangiform mechanics of vertebrate fish and aquatic mammals. An ostensible reason for the prevalence of this mode is its effectiveness when either resistive (viscous) or reactive (inertial) forces are used in the lateral pushes to achieve forward motion. Less well understood are the interactive roles of viscous and inertial forces in moderate Reynolds number locomotion. Lighthill [12] hypothesized that the thrust-producing mechanism is primarily reactive, and based his elongated body theory on the inertial force produced by the added mass. Viscosity was deemed important only as a contributor to drag, which was estimated from limp fish. A recent investigation of inviscid swimming by Kanso *et al* [9] has clearly shown the potential for net displacement with reliance on inertial forces alone. Using particle image velocimetry of swimming fish, Wolfgang *et al* [17] revealed that vortical structures shed over the length of the body may be actively manipulated to improve the swimming efficiency. Therefore, more work is necessary to clarify the role of vorticity, in order to exploit it in biologically inspired technology.

In this work, numerical simulations conducted with the viscous vortex particle method (VVPM) [6] are used to compute the fluid dynamics of a simple model for undulatory locomotion, a two-dimensional system of three linked ellipses. The high-fidelity method solves the incompressible Navier–Stokes equations by focusing on the creation, diffusion and convection of vorticity via the use of computational particles. A novel extension of the method to dynamically coupled problems, which exploits the physical connection between vorticity creation and body motion, is presented in this work. The motion of the body is simultaneously solved for with the motion of the fluid, allowing the exploration of free swimming. Thus, while the angles between the links are prescribed, the evolution of the position and orientation of the system is determined during the course of the simulation.

The results in this paper are preliminary and are intended to demonstrate the potential of the VVPM—when coupled with the body dynamics—for shedding new light on the basic mechanics of biolocomotion in fluids. This paper represents an initial step in an ongoing effort to understand wake–body interactions and motion planning in biolocomotion, and identify energy efficiency principles in this context. The central thesis of this work is that these issues can only be rigorously addressed if the actual self-propulsion of the system is part of the solution. It has become conventional to analyze locomotion in fluids by holding the system center of mass fixed and subjecting it to a constant free stream that balances the mean drag and thrust. This transformation presumes a steadiness in the forward locomotion speed; however, the unsteady component of the motion may be important [1, 15]. More importantly, there is no clear way to simulate maneuvering in the body-fixed reference frame. With these issues in mind, the numerical methodology employed in the present work has been constructed with special emphasis on the physical mechanics of fluid–body coupling.

It is important to note that the system analyzed in this work—three linked rigid bodies—is not meant to be representative of an actual fish, but instead, an abstraction of basic biomorphic locomotion. The system is designed so that its own dynamics are simple to describe, and so that it can be practically constructed (in future work) for experimental validation of the computational tools. The same system was explored in an inviscid medium by Kanso *et al* [9], and a robotic system with similar geometry was explored experimentally by Burdick and co-workers [14].

The basic numerical methodology is described in section 2. Results of swimming at two different Reynolds numbers are presented in section 3, and compared with the inviscid result of Kanso *et al* [9].

2. Methodology

2.1. Computation of fluid dynamics

An overview of the viscous vortex particle method (VVPM) is given in this section. For further details, the reader is referred to previous work [3, 6]. In the VVPM, the Navier–Stokes equations are discretized by N_v regularized particles, or *blobs*, of vorticity. This discretization is in contrast to more conventional grid-based treatments, such as finite difference or finite element methods, which interpolate the field quantities between fixed points or inside polygonal elements. The particles convect with the local velocity field, which ensures their automatic adaptivity to the flow. In a sense, this approach can be thought of as a 'moving grid', though the term 'grid' implies a reliance on connectivity between neighboring computational elements. Though the particles are initially arranged at the vertices of a Cartesian grid with uniform spacing Δx, the connectivity between grid points is immaterial.

The time-varying vorticity field is represented in terms of particles as

$$\omega(\mathbf{x}, t) = \sum_{p=1}^{N_v} V_p \omega_p(t) \zeta_\varepsilon(\mathbf{x} - \mathbf{x}_p(t)), \tag{1}$$

where V_p is the volume of particle p, which, for these two-dimensional problems, is Δx^2; $\mathbf{x}_p$ and ω_p are the position and vorticity associated with particle p, respectively; and ζ_ε is the regularization kernel, which decays rapidly beyond distance ε from the center of the particle. Each blob is represented by a second-order-accurate Gaussian cutoff function, evaluated efficiently from a look-up table. Equation (1) therefore represents an interpolation of the vorticity field by overlapping blobs.

The coupled fluid and body dynamics are solved with a fractional stepping procedure. In the first half-step of each time increment, the positions and strengths of the particles evolve according to the discretized convection and diffusion operations in the Navier–Stokes equations, respectively:

$$\frac{\mathrm{d}\mathbf{x}_p}{\mathrm{d}t} = \mathbf{u}(\mathbf{x}_p, t), \tag{2}$$

$$\frac{\mathrm{d}\omega_p}{\mathrm{d}t} = \frac{\nu}{\varepsilon^2} \sum_{q=1}^{N_v} V_q (\omega_p - \omega_q) \eta_\varepsilon(\mathbf{x}_p - \mathbf{x}_q). \tag{3}$$

The second equation is the particle-discretized version of the two-dimensional vorticity transport equation, $\mathrm{d}\omega/\mathrm{d}t = \nu\nabla^2\omega$ [4, 7], in a fluid with kinematic viscosity ν. The summation operator employs a smooth kernel, η, which weights the interactions between nearby particles by their separation distance; a second-order-accurate Gaussian function is used in this work.

The entire state of an incompressible flow can be determined from the vorticity and instantaneous body motion. Each vortex particle induces a circumferential velocity field around it, and the entire velocity field, $\mathbf{u}$, can be reconstructed by the composition of all particles' contributions. The vorticity contained inside each rigid body, $2\Omega_j$, and bound to the vortex sheet lying on each surface, also contributes to this velocity. Thus, each particle moves under the influence of every other particle, and a fast adaptive multipole method [2] is used to accelerate this $O\left(N_v^2\right)$ operation to $O(N_v)$. Equations (2) and (3) are integrated with a fourth-order Runge–Kutta method.

The no-slip condition is not enforced during this first half-step, and the resulting vorticity field, $\tilde{\omega}^{n+1}$, must be corrected in order to eliminate the spurious slip velocity. This correction is carried out in the second half-step by identifying the equivalent vortex sheet on the surface and fluxing it into the fluid. The slip velocity is thereby annihilated by this so-called Lighthill creation algorithm [10, 13]. In practice, the strength distribution, γ, of the surface vortex sheet is solved for with a conventional boundary element method. The vortex sheet is diffused into the fluid with the Neumann boundary condition $-\nu\partial\omega/\partial n = \gamma/\Delta t$, where the normal direction is into the fluid. The method utilizes a semi-analytical scheme developed by Leonard *et al* [11], in which the vorticity fluxed over a time increment $[0, \Delta t]$ from each boundary element is parceled to adjacent vortex particles. The final vorticity at the

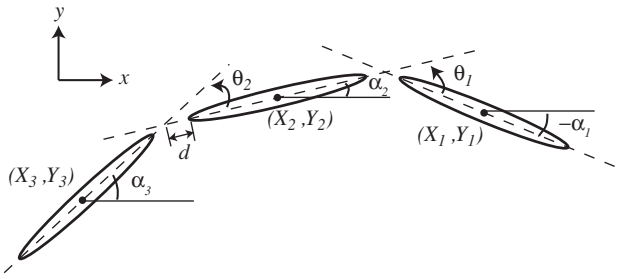

Figure 1. Schematic diagram of three-linkage fish.

end of the interval is composed of the intermediate field and the newly diffused one, $\omega^{n+1} = \tilde{\omega}^{n+1} + \Delta\omega^{n+1}$.

We can develop expressions for the fluid force and moment on each body in terms of the surface vorticity and vorticity flux. The configuration of body j is described by its centroid position $\mathbf{X}_j = (X_j, Y_j)$ and its angle α_j, as shown in figure 1; the respective rates of change are $\mathbf{U}_j = (U_j, V_j)$ and Ω_j. The fluid force components on body j are expressed as contour integrals around the perimeter S_j,

$$F^f_{x,j} = \mu \oint_{S_j} \left[(y(s) - Y_j)\frac{\partial \omega}{\partial n}(s) - n_y(s)\omega(s) \right] \mathrm{d}s + \rho_f A_j \dot{U}_j, \tag{4}$$

$$F^f_{y,j} = -\mu \oint_{S_j} \left[(x(s) - X_j)\frac{\partial \omega}{\partial n}(s) - n_x(s)\omega(s) \right] \mathrm{d}s + \rho_f A_j \dot{V}_j, \tag{5}$$

where (n_x, n_y) are the components of the local normal vector pointing into the fluid, $\mathbf{x}(s) = (x(s), y(s))$ are the parameterized coordinates of the body contour, A_j is the area of the body and μ and ρ_f are the dynamic viscosity and density of the fluid. The $\dot{(\ )}$ denotes differentiation with respect to time. The first term in the integral, together with the final inertial term, accounts for the effect of pressure; the second term represents the effect of the viscous shear stress. The fluid dynamic moment on body j about its centroid is

$$M^f_j = -\mu \oint_{S_j} \left\{ \frac{1}{2}|\mathbf{x}(s) - \mathbf{X}_j)|^2 \frac{\partial \omega}{\partial n}(s) - [(x(s) - X_j)n_y(s) - (y(s) - Y_j)n_x(s)]\omega(s) \right\} \mathrm{d}s - 4\mu A_j \Omega_j + 2\rho_f B_j \dot{\Omega}_j, \tag{6}$$

where B_j is the second area moment of body j. Note that in all expressions, (4)–(6), the vorticity flux can be replaced with the vortex sheet strength by using the relation $\mu\partial\omega/\partial n = -\rho_f \gamma/\Delta t$.

2.2. Body dynamics and fluid–body coupling

For coupled problems, as in the free swimming of an articulated body, the second half-step procedure is carried out simultaneously with the update of the body configuration. The rationale for this simultaneous procedure arises from the physical interdependence of vorticity production and body motion; the force and moment on the bodies are computed from the vorticity and vorticity flux, the individual body dynamics are influenced by this force and moment and the spurious slip left by the resulting body motion translates into vorticity flux. Thus, to close out each time increment, we seek the body motion and vorticity flux that are consistent with each other, via the reaction force between fluid and body.

Each of the bodies in the linked system obeys Newton's second law of motion. However, because of the linkage constraints, the configuration of the entire system can be expressed in terms of the configuration of a reference body (body 1, for instance) and the instantaneous hinge angles, and the dynamical equations are formulated accordingly. Let $\mathcal{X}$ denote the three-dimensional configuration vector of the reference body, $(X_1, Y_1, \alpha_1)^T$, and $\mathcal{U}$ the rate of change of this vector, $(U_1, V_1, \Omega_1)^T$. The six-dimensional state vector is denoted by $\mathcal{Z} = (X_1, Y_1, \alpha_1, U_1, V_1, \Omega_1)^T$ and Θ is the two-dimensional hinge angle vector $(\theta_1, \theta_2)^T$.

In the free swimming problem, the shape of the system is prescribed, and the resulting changes in position and orientation are a consequence of the coupled equations of fluid–body motion. In analogy, a fish can only control its own shape, through muscular actuation, and has no direct control over its position in space. Thus, Θ is a prescribed 'forcing' function for the dynamics. The dynamical equations for the system can be written in s matrix form as

$$\dot{\mathcal{X}} = \mathcal{U}, \tag{7}$$

$$\dot{\mathcal{U}} = \mathbb{M}^{-1}(-\mathbb{M}_\theta \ddot{\Theta} + \mathcal{J} + \mathcal{F}^f), \tag{8}$$

where $\mathbb{M}$ and $\mathbb{M}_\theta$ are inertial matrices, $\mathcal{J}$ contains the centrifugal terms and $\mathcal{F}^f$ the fluid forces and moments:

$$\mathcal{F}^f = \sum_j \begin{pmatrix} F^f_{x,j} \\ F^f_{y,j} \\ M^f_j - (Y_j - Y_1)F^f_{x,j} + (X_j - X_1)F^f_{y,j} \end{pmatrix} \tag{9}$$

We can generically write the dynamical equations (7) and (8) as

$$\dot{\mathcal{Z}} = \mathcal{F}(\mathcal{Z}, \dot{\mathcal{Z}}, \Theta, \gamma, \omega). \tag{10}$$

The arguments on the right-hand side reflect the dependences of the body dynamics on the state of the fluid, via the force and moment. The dynamical equations are integrated with a predictor–corrector scheme; the predictor is a first-order Adams–Bashforth method and the corrector is a second-order Adams–Moulton method. At the end of the first half-step of each time interval the body system has state $\mathcal{Z}^n$, the fluid has vorticity $\tilde{\omega}^{n+1}$ and the rate-of-change vector is $\mathcal{F}^n$. We seek to update these to $\mathcal{Z}^{n+1}$, ω^{n+1} and $\mathcal{F}^{n+1}$, respectively, with zero slip between body and fluid. The procedure is written algorithmically as follows:

(i) *Predictor:*

$$\mathcal{Z}^{n+1}_{(0)} = \mathcal{Z}^n + \Delta t \mathcal{F}^n \Longrightarrow \gamma_{(0)}, \Delta\omega^{n+1}_{(0)} \tag{11}$$

$$\dot{\mathcal{Z}}^{n+1}_{(0)} = 0 \tag{12}$$

$$\mathcal{F}^{n+1}_{(0)} = \mathcal{F}\big(\mathcal{Z}^{n+1}_{(0)}, \dot{\mathcal{Z}}^{n+1}_{(0)}, \Theta^{n+1}, \gamma_{(0)}, \tilde{\omega}^{n+1} + \Delta\omega^{n+1}_{(0)}\big). \tag{13}$$

(ii) *Corrector* (*m*th iteration):

$$\mathcal{Z}^{n+1}_{(m+1)} = \mathcal{Z}^n + \frac{1}{2}\Delta t\left(\mathcal{F}^n + \mathcal{F}^{n+1}_{(m)}\right) \tag{14}$$
$$\Longrightarrow \gamma_{(m+1)},\ \Delta\omega^{n+1}_{(m+1)}$$

$$\dot{\mathcal{Z}}^{n+1}_{(m+1)} = \mathcal{F}^{n+1}_{(m)} \tag{15}$$

$$\mathcal{F}^{n+1}_{(m+1)} = \mathcal{F}\left(\mathcal{Z}^{n+1}_{(m+1)}, \dot{\mathcal{Z}}^{n+1}_{(m+1)}, \Theta^{n+1}, \gamma_{(m+1)}, \tilde{\omega}^{n+1} + \Delta\omega^{n+1}_{(m+1)}\right). \tag{16}$$

The corrector step is iterated at most three times. Note that the double right arrow denotes that the updated body configuration is used to solve for the spurious vortex sheet strength and diffuse it into the flow. It should be noted that no convergence proof exists for this coupling procedure, nor has one been attempted; however, experience has shown that the procedure converges numerically. Further details of this coupling procedure can be found in [5].

3. Results

The focus of this work consists of a linked system of three identical elliptical bodies, each of length c and aspect ratio 10. The motions of the rigid links are constrained by virtual hinges that are a fixed distance, $d = 0.2c$, from the adjacent ellipses (see figure 1). The gaps between the bodies are 'open', in the sense that fluid is permitted to traverse the system. These gaps are left to simplify the numerics. This configuration serves only as an abstraction of basic undulatory kinematics, and is not meant as a realistic model of an actual fish. It is noted that the disjoint bodies do bear some resemblance to a cross-sectional view of dorsal fins on some fish (e.g. the bluegill sunfish [8]), but these fins have a three-dimensional structure that is absent from the present system.

In the present work, the hinge angles of the three-linkage system are prescribed with

$$\theta_1 = \Omega_m \cos(t - t_0), \tag{17}$$
$$\theta_2 = \Omega_m \cos(t - t_0 - \pi/2), \tag{18}$$

with $\Omega_m = 1$ and $t_0 = \pi$. These inputs represent a lowest order form of undulatory kinematics employed by, for example, anguilliform fish. The inviscid response of the same system to these control inputs was analyzed by Kanso *et al* [9]. In that work, the absence of dissipation allowed the dynamics of the fish and inviscid fluid to be treated in a unified fashion through a single Lagrangian. Such an analysis is not possible in a viscous flow, where energy is continually dissipated.

The VVPM-computed motion of the three-linkage fish in a viscous medium is depicted in figure 2. The Reynolds number of this system, based on the maximum hinge rotation rate and the chord of each body, $\Omega_m c^2/\nu$, is 1000. The system propels itself in a mean direction 20° clockwise from the positive horizontal axis, at a speed of approximately 0.4 body lengths per undulatory period. The pattern of vortex shedding during

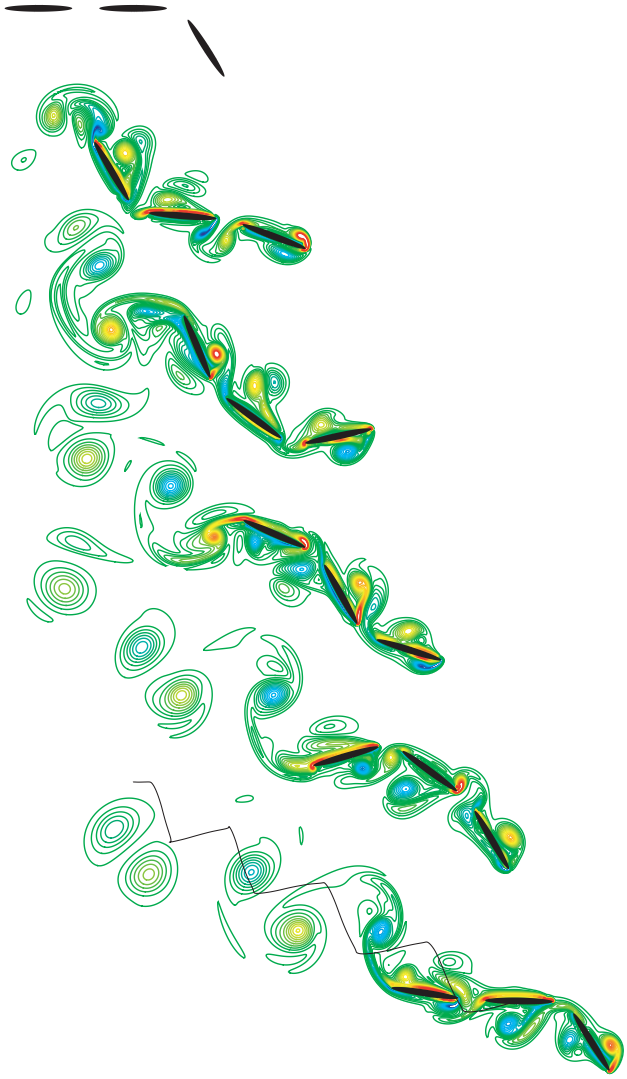

Figure 2. Vorticity field contours at six instants during swimming of three-linkage fish at $Re = 1000$. From top to bottom, $t/T = 0, 0.796, 1.592, 2.387, 3.183$ and 4. Trajectory of central body shown for reference at final instant.

the swimming is complicated by the internal edges of the constituent bodies. Each lateral heave of the fish produces a small vortex dipole on the opposite side. These dipoles are reabsorbed by the boundary layer along the posterior portion of the fish; the same is true for vorticity shed from the leading edge of the fish.

The pitching and heaving tail of the fish produces a wake pattern of vortices of alternating sign. The pattern configuration is reminiscent of a reverse Karman vortex street, which has been observed in the wakes of fish and robotic swimmers [16]. However, this canonical wake is more clearly apparent when the amplitude of the tail motion is large, as in the carangiform mechanics of fish such as trout.

The effectiveness of these mechanics for achieving forward locomotion depends on the viscosity in the surrounding fluid. This is clearly apparent in figure 3, which depicts the trajectories of the central body of the fish after

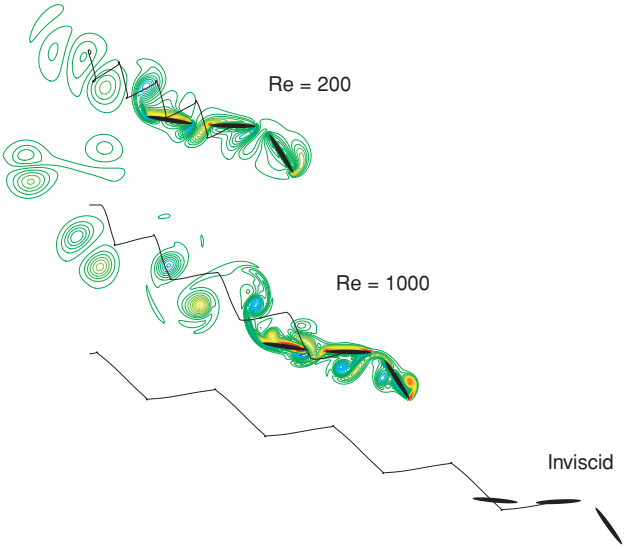

Figure 3. Vorticity field and trajectories of three-linkage fish after four undulation cycles, at two different Reynolds numbers, compared with the inviscid trajectory of Kanso *et al* [9].

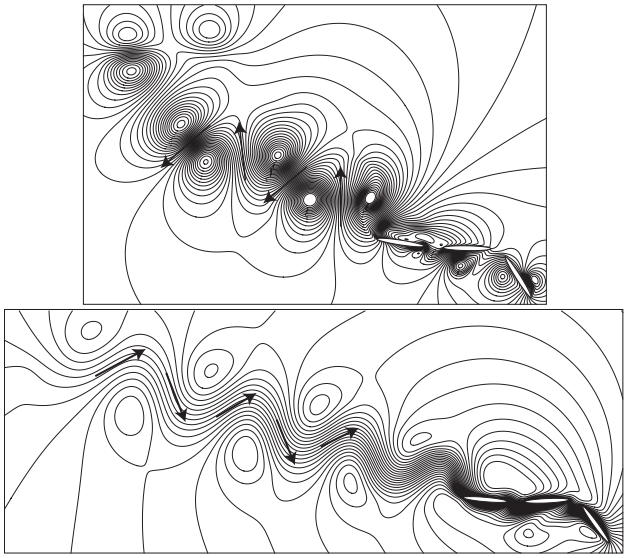

Figure 4. Instantaneous streamline patterns for free swimming fish at $Re = 1000$ (top) and system with prescribed motion at $Re = 200$ (bottom).

four undulatory cycles at two different Reynolds numbers; the trajectory of the inviscid swimmer, computed by Kanso *et al* [9], is included for reference. At the smaller Reynolds number, the fish swims approximately half as far as in the less viscous case. Furthermore, the wake vortices are more tightly bunched, since less distance is traveled between shedding instants. The inviscid swimmer travels approximately 0.7 body lengths per undulatory cycle, nearly $2/3$ faster than the highest Reynolds number case shown.

A question naturally arises from this analysis: is the speed of locomotion fastest for the inviscid swimmer? By Kelvin's minimum-energy theorem, the fish must exert the least amount of work in the inviscid case. However, this does not, in itself, imply that viscous swimmers must necessarily swim slower. Another consequence of inviscid mechanics is that the fluid and body motion cease immediately when the control inputs are impulsively stopped. Viscous flows, on the other hand, are subject to 'drift,' so the residual vorticity in the fluid can lead to motion in the fluid–body system even after the swimmer has stopped exertion. That is, energy can be usefully extracted from the vortical flow. Thus, it is possible that the three-linkage fish may swim faster than the inviscid case in a medium that is less viscous than the ones considered here. We are currently investigating this.

It is interesting to examine the differences in wake topology between a free swimming fish and one that is 'pulled' at an arbitrary velocity. This comparison is shown in figure 4, which depicts the instantaneous streamline patterns for two cases: the first is the free swimmer at $Re = 1000$; the second corresponds to a fish with a prescribed motion (at $Re = 200$) adopted from the inviscid trajectory calculated by Kanso *et al* [9]. In the free swimming case, the wake streamline pattern clarifies the reverse Karman vortex street seen in figure 2. The velocity vectors have a slight rearward orientation, consistent with the thrust that propels the fish. In contrast, the streamline pattern for the other case corresponds to a drag wake, in the form of a classical vortex street and the associated momentum defect.

4. Conclusions

In this work, the viscous vortex particle method has been used to simulate the free swimming of a three-linkage 'fish' undergoing undulatory mechanics. A novel fluid–body coupling algorithm has been presented which exploits the physical relationship between vorticity creation and body motion. Vorticity is shed into a sequence of alternating sign vortices that is indicative of a thrust-producing wake. The trajectory and speed were compared with results for swimming in an inviscid medium. It was found that, in the cases analyzed, viscosity has a predominantly dissipative role. An increase in Reynolds number leads to a corresponding increase in the forward swimming speed, which is lower than the inviscid speed with the same prescribed undulatory kinematics. Though this result seems intuitive, the comparison has never been made before. More analysis at higher Reynolds numbers must be carried out to determine whether there exists a maximum mean forward speed at nonzero viscosity for this set of kinematics. In future work we will also examine the effect of various hinge control inputs on the maneuverability of the fish, and investigate the interaction of the fish with ambient vorticity (for example, from the wake of another fish) for improved efficiency.

References

[1] Carling J, Williams T L and Bowtell G 1998 Self-propelled anguilliform swimming: simultaneous solutions of the two-dimensional Navier–Stokes equations and Newton's laws of motion *J. Exp. Biol.* **201** 3143–66

[2] Carrier J, Greengard L and Rokhlin V 1988 A fast adaptive multipole algorithm for particle simulations *SIAM J. Sci. Stat. Comput.* **9** 669–86
[3] Cottet G-H and Koumoutsakos P 2000 *Vortex Methods: Theory and Practice* (Cambridge: Cambridge University Press)
[4] Degond P and Mas-Gallic S 1989 The weighted particle method for convection–diffusion equations: I. The case of an isotropic viscosity *Math. Comp.* **53** 485–507
[5] Eldredge J D 2007 Vorticity-based numerical simulations of dynamically coupled fluid–body interactions. In preparation
[6] Eldredge J D 2006 Numerical simulation of the fluid dynamics of 2D rigid body motion with the vortex particle method *J. Comput. Phys.* doi:10.1016/j.jcp.2006.06.038
[7] Eldredge J D, Leonard A and Colonius T 2002 A general deterministic treatment of derivatives in particle methods *J. Comput. Phys.* **180** 686–709
[8] Fish F E and Lauder G V 2006 Passive and active flow control by swimming fishes and mammals *Ann. Rev. Fluid Mech.* **38** 193–224
[9] Kanso E, Marsden J E, Rowley C W and Melli-Huber J 2005 Locomotion of articulated bodies in a perfect fluid *J. Nonlinear Sci.* **15** 255–89
[10] Koumoutsakos P, Leonard A and Pépin F 1994 Boundary conditions for viscous vortex methods *J. Comput. Phys.* **113** 52–61
[11] Leonard A, Shiels D, Salmon J K, Winckelmans G S and Ploumhans P 1997 Recent advances in high resolution vortex methods for incompressible flows *AIAA Paper* 97-2108
[12] Lighthill M J 1960 Note on the swimming of slender fish *J. Fluid Mech.* **9** 305–17
[13] Lighthill M J 1961 Introduction: boundary layer theory *Laminar Boundary Layers* ed L Rosenhead (Oxford: Clarendon)
[14] Mason R and Burdick J W 2000 Experiments in carangiform robotic fish locomotion *IEEE Int. Conf. on Robotics and Automation*
[15] Schultz W W and Webb P W 2002 Power requirements of swimming: do new methods resolve old questions? *Integr. Comp. Biol.* **42** 1018–25
[16] Triantafyllou M S, Triantafyllou G S and Yue D K P 2000 Hydrodynamics of fishlike swimming *Ann. Rev. Fluid Mech.* **32** 33–53
[17] Wolfgang M J, Anderson J M, Grosenbaugh M A, Yue D K P and Triantafyllou M S 1999 Near-body flow dynamics in swimming fish *J. Exp. Biol.* **202** 2303–27